Chemical Science

ROYAL SOCIETY OF CHEMISTRY

EDGE ARTICLE

View Article Online
View Journal | View Issue

Cite this: *Chem. Sci.*, 2022, **13**, 11382

All publication charges for this article have been paid for by the Royal Society of Chemistry

Received 19th July 2022
Accepted 5th September 2022

DOI: 10.1039/d2sc04042e

rsc.li/chemical-science

Synthesis, structure and reactivity of μ_3-SnH capped trinuclear nickel cluster†

Nicole A. Torquato,[a] Joseph M. Palasz,[a] Quentin C. Bertrand,[b] Felix M. Brunner,[a] Thomas Chan,[a] Milan Gembicky,[a] Anthony A. Mrse[a] and Clifford P. Kubiak *[a]

Treatment of the trichlorotin-capped trinuclear nickel cluster, $[Ni_3(dppm)_3(\mu_3\text{-}Cl)(\mu_3\text{-}SnCl_3)]$, **1**, with 4 eq. $NaHB(Et)_3$ yields a μ_3-SnH capped trinuclear nickel cluster, $[Ni_3(dppm)_3(\mu_3\text{-}H)(\mu_3\text{-}SnH)]$, **2** [dppm = bis(diphenylphosphino)methane]. Single-crystal X-ray diffraction, nuclear magnetic resonance (NMR) spectroscopy, and computational studies together support that cluster **2** is a divalent tin hydride. Complex **2** displays a wide range of reactivity including oxidative addition of bromoethane across the Sn center. Addition of 1 eq. iodoethane to complex **2** releases H_2 (g) and generates an ethyltin-capped nickel cluster with a μ_3-iodide, $[Ni_3(dppm)_3(\mu_3\text{-}I)(\mu_3\text{-}Sn(CH_2CH_3))]$, **4**. Notably, insertion of alkynes into the Sn–H bond of **2** can be achieved *via* addition of 1 eq. 1-hexyne to generate the 1-hexen-2-yl-tin-capped nickel cluster, $[Ni_3(dppm)_3(\mu_3H)(\mu_3\text{-}Sn(C_6H_{11}))]$, **5**. Addition of H_2 (g) to **5** regenerates the starting material, **2**, and hexane. The formally 44-electron cluster **2** also displays significant redox chemistry with two reversible one-electron oxidations (E = −1.3 V, −0.8 V *vs.* $Fc^{0/+}$) and one-electron reduction process (E = −2.7 V *vs.* $Fc^{0/+}$) observed by cyclic voltammetry.

Introduction

Tin hydrides have been widely employed in stoichiometric and catalytic hydrogen atom transfer to a diverse range of substrates.[1,2] Industrially relevant tin hydrides predominately feature tin in the +4 oxidation state. However, recent advances in group 14 hydride chemistry have introduced a range of tin hydride species formally in the +2 oxidation state that enable new reactivity profiles and pathways.[1,3] Over the past 20 years, seminal studies by Power and co-workers have demonstrated the synthesis, isolation, and structural characterization of low-valent Sn, Ge, and Pb hydrides.[4–8] These studies have led to multiple advances in main group reactivity, such as aromatic C–F activation, C–H activation, hydrostannylation chemistry, and catalytic hydroboration.[9–13] Furthermore, recent studies have revealed new functionalities for tin(II) species including reversible coordination of H_2, coordination of NH_3 and N–H activation, and oxidative addition of H_2, H_2O, and silyl and boryl Sn^{IV} species.[14,15] In an effort to change the electronics and structural platform for tin hydride complexes, there have been reports of tin hydride complexes coordinated to transition metals, featuring tin in the +2 oxidation state, utilizing Lewis base/Lewis acid pairs for stabilization.[16–21] Overall, these advancements in the tin chemistry platform specifically regarding the production of low valent and highly reduced tin species have led to the observation of transition-metal like reactivity of tin, including activation of small and unsaturated molecules.[22] In an effort to expand on the known structural and reaction chemistry of tin, we sought to investigate the impacts of supporting different tin functional groups on polynuclear transition metal clusters.[23–25] Herein, we describe the synthesis, structure, and reactivity of a divalent Sn hydride capped trinuclear nickel cluster, $[Ni_3(dppm)_3(\mu_3\text{-}H)(\mu_3\text{-}SnH)]$, **2** [dppm = bis(diphenylphosphino)methane]. Complex **2**, displays a wide range of reactivity, including oxidative addition of alkyl halides and alkyne insertion with subsequent hydrogenation.

Results and discussion

The synthesis and structural determination of a trichlorostannyl-capped cluster $[Ni_3(dppm)_3(\mu_3\text{-}Cl)(\mu_3\text{-}SnCl_3)]$ (**1**) has been reported previously.[26] Treatment of **1** with 4 eq. $NaB(Et)_3H$ at room temperature liberates H_2 and affords **2** in 88% yield (Scheme 1). This complex was characterized by X-ray crystallography, nuclear magnetic resonance (NMR) spectroscopy, and cyclic voltammetry. DFT calculations were also used to investigate the electronic structure.

Vapor diffusion of diethyl ether into a THF solution of **2** at −35 °C resulted in brownish-red X-ray quality crystals. X-ray diffraction revealed that cluster **2** crystallized in the triclinic space group $P\bar{1}$ and features a μ_3-Sn atom capping a triangular face consisting of three nickel atoms supported by three

[a]*Department of Chemistry and Biochemistry, University of California, San Diego, 9500 Gilman Dr, La Jolla, CA, 92093, USA. E-mail: ckubiak@ucsd.edu*

[b]*Department of Chemistry, Yale University, New Haven, CT 06520, USA*

† Electronic supplementary information (ESI) available. CCDC 2173131, 2169137, 2169160 and 2102266. For ESI and crystallographic data in CIF or other electronic format see https://doi.org/10.1039/d2sc04042e

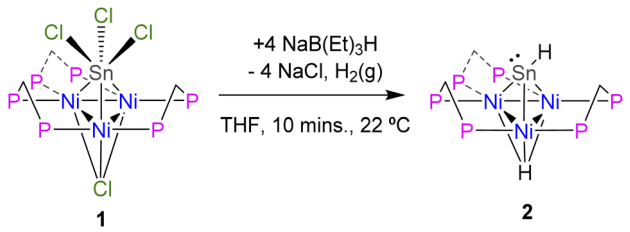

1 2

Scheme 1 Synthesis of $[Ni_3(dppm)_3(\mu_3\text{-}H)(\mu_3\text{-}SnH)]$, **2**.

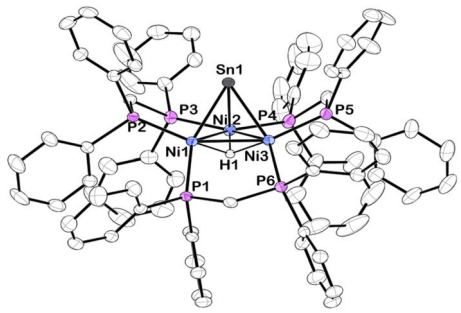

Fig. 1 Solid-state structure of **2** as determined by single-crystal X-ray diffraction. Thermal ellipsoids were set at the 50% probability level. A diethyl ether molecule and carbon bound hydrogens were omitted for clarity. The hydride attached to Sn was not precisely located.

bridging dppm ligands (Fig. 1). Although the Sn–H hydrogen atom in **2** could not be precisely located in the difference electron-density map, the Sn–H linkage was unequivocally confirmed by ^{1}H and ^{119}Sn NMR spectroscopy (*vide infra*). Density functional theory (DFT) calculations and natural bond orbital (NBO) analysis also support this structural assignment (see ESI† for details).

Compared to **1**, **2** exhibits substantially shorter Sn–Ni bond distances and considerably longer Ni–Ni bond distances (Table 1). While many low-valent Sn-hydrides form dimers,[3,4,9] **2** does not, likely as a result of the trinuclear $Ni_3(dppm)_3$ framework providing considerable steric bulk, an effect seen in other monomeric Sn–H complexes.[27,28] The structure of **2** shows slight variations in Ni–Sn bond distances. Additionally, the Ni_1–Ni_3 bond distance is significantly shortened in comparison to the other Ni–Ni bonds (Fig. 1 and Table 1). This implies that, in the solid-state, the μ_3 binding of the Sn–H is not entirely symmetric, and the interactions of Sn–H may be more localized on one nickel center. Similar variations in Ni–Sn bond distances are seen in the starting material, **1**.[25,26] These structural features are also observed in the results of DFT calculations. DFT and natural bond order (NBO) analysis for complex **2** (B3LYP/LANL2DZ) reveal that the Sn–H interacts principally with one nickel atom (Fig. 2, see also ESI†).

Further details of the molecular and electronic structure were elucidated by ^{31}P, ^{1}H, and ^{119}Sn NMR spectroscopy. The ^{31}P NMR spectroscopy of **2** in benzene-d_6 revealed symmetrical binding of the μ_3-SnH and μ_3-H capping groups on the NMR

Table 1 Selected bond distances and angles of **1**, **2**, **3**, **4** and **5**

Bond length [Å]/angle [°]	1	2	3	4	5
Ni1–Ni2	2.4593(18)	2.7445(6)	2.4104(9)	2.6840(5)	2.5011(10)
Ni1–Ni3	2.4829(18)	2.4449(5)	2.4020(9)	2.8886(5)	2.5285(10)
Ni2–Ni3	2.4825(16)	2.7315(6)	2.3858(9)	2.8227(5)	2.6655(11)
Sn1–Ni1	2.6118(14)	2.5187(5)	2.7261(8)	2.4423(4)	2.4324(8)
Sn1–Ni2	2.5960(16)	2.5502(5)	2.5716(7)	2.4419(4)	2.5282(8)
Sn1–Ni3	2.6185(16)	2.5348(5)	2.7447(7)	2.4607(4)	2.4724(8)
∠C–Sn–Ni1				143.57(8)	162.02(16)
∠C–Sn–Ni2				140.24(8)	136.59(17)
∠C–Sn–Ni3				132.11(8)	125.91(16)

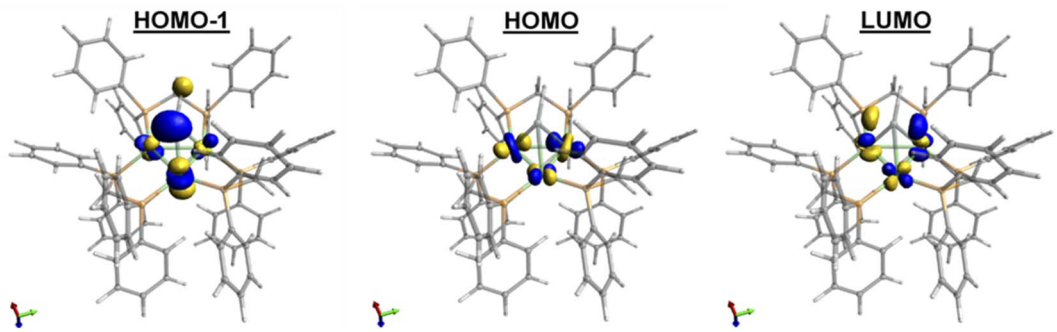

Fig. 2 Computed molecular orbitals of **2**, utilizing a B3LYP basis set and LANL2DZ functional showing the two highest energy occupied orbitals (HOMO−1 and HOMO) and the lowest energy unoccupied orbital (LUMO).

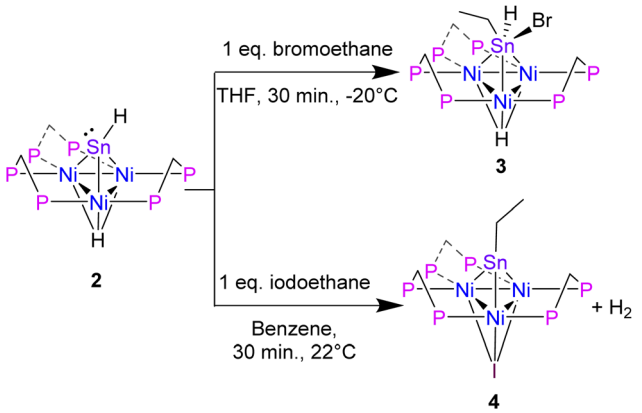

Scheme 2 Synthesis of **3** and **4**.

Table 2 Selected chemical shifts and $^{1}J_{(Sn-H)}$ in benzene-d_6 of **2**,**3**,**4**, and **5**

	^{31}P, δ (ppm)	Ni–H, δ (ppm)	Sn–H, δ (ppm)	^{119}Sn, δ (ppm)	$^{1}J_{(Sn-H)}$ (Hz)
2	23.4	−0.86	−0.42	2939.4	346.7
3	4.2	−4.80	8.77	248.0	993.6
4	34.1			2115.1	
5	31.0	3.54–3.62		1837.8	

timescale as demonstrated by an isolated sharp singlet resonance at 23.4 ppm. The Ni–H resonance was located in the ^{1}H NMR at −0.86 ppm and it appears as a heptet, featuring significant two-bond coupling ($^{2}J_{P-H}$) to the six phosphorus atoms coordinated to the nickel atoms. In addition, the Sn–H ^{1}H NMR resonance was located at −0.42 ppm and it appears as a singlet. The assignment of this resonance as that belonging to the hydrogen-bound Sn was evidenced by the proton-coupled ^{119}Sn NMR spectrum which, at room temperature, features a doublet at 2939.4 ppm (see ESI: S4†). The ^{1}H decoupled ^{119}Sn NMR spectrum contained a singlet resonance, indicating that there is one hydrogen atom bound to Sn, which is also further confirmed by integration of the peaks in the ^{1}H NMR spectrum.

Satellite peaks arising from coupling of hydrogen to the ^{117}Sn and ^{119}Sn nuclei with $^{1}J_{(Sn-H)}$ values near 1900 Hz are normally observed for tetravalent Sn(IV) hydrides.[3,29,30] In contrast, divalent Sn(II) hydride complexes typically exhibit much smaller coupling constants ($^{1}J_{(Sn-H)}$ *ca.* 100 Hz) because in these Sn(II) hydrides most of the s-orbital electron density is localized to the lone pair on Sn.[4,31–33] The $^{1}J_{(117/119Sn-1H)}$ coupling constant of **2** was found to be 360 Hz, consistent with a divalent Sn center. This assignment is corroborated by NBO analysis, which predicts that the Sn hybridization used to form the Sn–H linkage in **2** has about 20% s-character at Sn. Furthermore, DFT analysis indicates the presence of a lone pair on Sn in the HOMO−1 (Fig. 2). In addition, preliminary Mössbauer results on **2** depict a +2 oxidation state Sn center. Overall, NMR, computational studies, and preliminary Mössbauer results suggest that the Sn can be considered as sp^2 hybridized with most of the s-orbital density localized on a lone pair on Sn.

To support experimentally the assignment of **2** as a Sn(II) hydride with a lone pair, we performed reactivity studies. Alkyl halides are known to undergo oxidative addition to Sn(II) complexes that feature a lone pair.[34] Addition of 1 eq. $BrCH_2CH_3$ to **2** in THF at −20 °C, results in the oxidative addition of $BrCH_2CH_3$ at the Sn center and formation of [Ni_3(dppm)$_3$(μ_3-H)(μ_3-Sn((Br)(H)(CH_2CH_3)))], **3** in 75% yield (Scheme 2).

The formation of **3** is characterized by a significant upfield shift in the ^{31}P NMR spectrum compared to **2**, with a resonance located at 4.2 ppm in benzene-d_6. As for the ^{1}H NMR signals, the Ni–H resonance shifts upfield to −4.70 appearing as a heptet, and the Sn–H resonance shifts downfield to 8.78 ppm, presumably a result of the close proximity to the Sn–Br bond. There is significant broadening in the ^{31}P and ^{1}H NMR spectra due to the break in symmetry from the three different functional groups attached to Sn. In comparison to **2**, the proton-coupled ^{119}Sn NMR of **3** depicts an upshifted doublet with a resonance located at 247.8 ppm and a $^{1}J_{(Sn-H)}$ = 993.6 Hz, suggesting a larger s orbital contribution from the Sn into the H atom bond (Table 2, also see ESI: S9†). The $^{1}J_{(Sn-H)}$ value of **3** is comparable to that reported by the Rivard group for a Sn(II) dihydride transition metal coordinated complex, IPr–SnH_2–$W(CO)_5$ (IPr = [(HCNAr′)$_2$C:]; Ar′ = 2,6-^{i}Pr$_2$C$_6$H$_3$).[16]

Vapor diffusion of pentane into a THF solution of **3** at −20 °C resulted in red colored X-ray quality crystals (Fig. 3). The hydride attached to Sn was not precisely located. There appears to be significant asymmetry of the μ_3-SnHBr(CH_2CH_3) binding

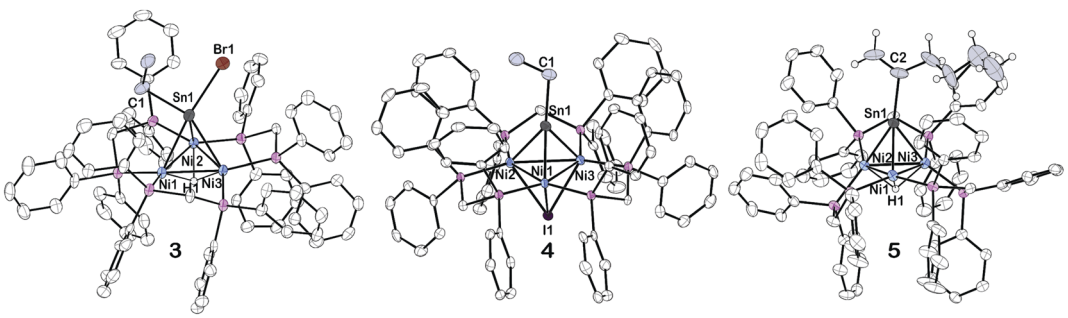

Fig. 3 Solid-state structure of **3**, **4** and **5** as determined by single-crystal X-ray diffraction. Thermal ellipsoids were set at the 50% probability level. A solvent molecule and carbon bound hydrogens were omitted for clarity. The hydride attached to tin was not precisely located in complex **3**. Carbons atoms on bis(diphenylphosphino)methane ligands are colored white, while those on Sn are colored grey.

to the trinuclear nickel core, suggested by the significant elongation of the Sn–Ni1 and Sn–Ni3 bonds *versus* the Sn–Ni2 bond (Table 1). Furthermore, the data indicates an overall shortening of the Ni–Ni bond distances more closely resembling that of cluster **1** than **2** (Table 1).

Surprisingly, in an analogous reaction to forming cluster **3**, treatment of **2** with 1 eq. ICH_2CH_3, releases H_2 and generates an CH_3CH_2Sn-capped, nickel cluster with a μ_3 iodide [Ni_3(dppm)$_3$(μ_3-I)(μ_3-Sn(CH_2CH_3))], **4**, in 94% yield (Scheme 2). The formation of **4**, is characterized by a significant downfield shift from the starting material in the ^{31}P NMR to 34.1 ppm in benzene-d_6, which is flanked by satellites arising from 2-bond coupling to the ^{119}Sn nuclei ($^2J_{(Sn,P)}$ = 98.8 Hz), while the ^{119}Sn NMR shifts upfield to 2115.14 ppm (Table 2, see ESI: S14†).

Layering of pentane over a benzene solution of **4** at 22 °C resulted in brownish-red X-ray quality crystals (Fig. 3). The Sn–Ni bond distances and the C–Sn–Ni bond angles reveal an almost linear binding orientation of the μ_3-SnCH_2CH_3 to the center of the trinuclear nickel core. Furthermore, the shortened Sn–Ni bond distances: 2.4423(4), 2.4419(4), and 2.4607(4), are of similar length to other transition metal coordinated stannylyne complexes in the literature, which primarily exhibit a linear arrangement unless there are considerable steric demands due to the ligand environment.[35–40] We will report separately results of Mössbauer spectroscopy and computational studies to support this assignment.

Hydrostannylation is a well-known transformation in organic chemistry.[41] Hydrostannylation utilizing tin(II) species has been demonstrated. These reactions feature transition metal and radical catalyst-free *cis*-hydrostannylation of the alkynes under mild conditions.[42–44] Therefore, it was of interest to evaluate the reactivity of complex **2** with alkynes. 1 eq. of 1-hexyne was added to **2** in a benzene solution, which resulted in insertion to yield 1-hexen-2-yl-Sn-capped nickel cluster [Ni_3(dppm)$_3$(μ_3-H)(μ_3-Sn(C_6H_{11}))], **5**, in 98% yield (Scheme 3). A study from the Power group demonstrated Sn(II) hydrostannylation of primary alkynes resulted in Sn binding to the terminal position.[42] However, complex **5** exhibits a distinct preference to bind to the secondary position.

The formation of **5**, is characterized by an upfield shift in the ^{31}P NMR to 31.0 ppm from the starting material, **2**. In comparison to **2**, an upshifted Ni–H resonance in the ^{1}H NMR was observed at −3.54 to −3.62 ppm, while the ^{119}Sn NMR resonance shifted upfield to 1837.8 ppm. Vapor diffusion of pentane into a diethyl ether solution of **5** at −20 °C results in brown X-ray quality crystals (Fig. 3). The μ_3-Sn(C_6H_{11}) features a significant bend from a 180-degree angle to the center of the three nickel clusters, suggesting the presence of a lone pair on the Sn, similar to cluster **2** (Table 1). This is supported by variations in the Sn–Ni bond distances in complex **5**, in contrast to **4**. Additionally, the Sn–Ni and Ni–Ni bond distances in **5** is similar to those of complex **2** (Table 1).

After isolating complex **5**, hydrogenation of the 1-hexen-2-yl fragment and regeneration of **2** was attempted. Upon addition of H_2 (*g*) to complex **5**, complex **2** and hexane are formed in 21% yield by ^{1}H NMR. In this process, an intermediate species is formed at −4.5 ppm *via* ^{31}P NMR and there is a shift in the Ni–H resonance to −6.2 ppm *via* ^{1}H NMR, before the regeneration of complex **2** (see ESI: S19–S21†). Thus far, this intermediate has proved elusive due to the chemical instability in solution. NMR stability studies of **5** in THF-d_8 at 22 °C found that 92% of the initial integration of ^{1}H NMR features were lost over 24 hours, leading to a variety of unidentified species (see ESI: S22 and S23†). Repeat studies in benzene-d_6 yielded similar conclusions. This is an unexpected result, as previous studies demonstrating tin(II) hydrostannylation of alkynes only studied the formation of stable tin alkene species and have not shown the hydrogenation chemistry of these products.[42–44] The literature indicates that, Sn has primarily been utilized as a stoichiometric reagent, however, this study demonstrates a platform that may lead to catalytic application of alkyne reduction by Sn–H utilizing H_2 (*g*).[41]

Finally, the oxidative addition chemistry revealed by the novel low valent μ_3-SnH capped trinuclear nickel cluster **2** raises the question of electronics pertaining to this species. Cyclic voltammetry (CV) of a solution of **2** in THF revealed two reversible, one-electron oxidations (at E = −0.8, −1.3 V *vs.* $[Cp_2Fe]^{0/+}$) and one partially-reversible one electron reduction process (E = −2.7 V *vs.* $[Cp_2Fe]^{0/+}$) (see ESI for CV: S27–S31†). Complex **2** is a formally 44-electron trinuclear cluster of the *closo* structural class and is therefore electronically deficient in accordance with Wade's rules.[45,46] To elucidate the nature of these oxidation events, we computed molecular orbitals of **2** (Fig. 2). Analysis of the computed MOs suggests that the oxidation events involve depleting electron density from the d-orbital based Ni–Ni antibonding interactions, thereby providing relief from antibonding instability. The reduction process is best described as the introduction of electron density into the LUMO, which features electron density shared between the Ni_3 core and Sn and d-orbital based Ni–Ni antibonding interactions. This is expected to increase Ni–Ni antibonding

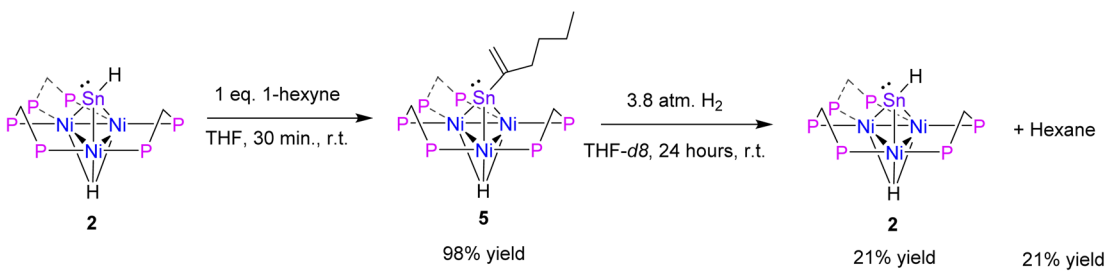

Scheme 3 Synthesis of [Ni_3(dppm)$_3$(μ_3-H)(μ_3-Sn)(C_6H_{11})], **5**, and hydrogenation to [Ni_3(dppm)$_3$(μ_3-H)(μ_3-SnH)], **2**.

instability in the complex, which is consistent with the partial irreversibility observed for the redox process observed in the CV. Together, the electrochemical and DFT results of **2** suggest frontier d-orbitals interactions centered at the Ni_3 core. Given that the coordination environment around the Ni_3 cluster does not allow for activation by the Ni_3 center, we propose these charge states may be mediated through the Sn center, potentially enabling the oxidative addition and unique hydrogenation chemistry displayed here.

Conclusion

In summary, this report describes the synthesis and structural analysis of a divalent Sn–H capped trinuclear nickel cluster. This cluster features three chemically reversible redox processes and may represent an example of a general and useful platform for isolating Sn–H species to investigate their electronic properties and chemical reactivity in greater detail. Cluster **2** displays a breadth of reactivity, including oxidative addition of alkyl halides and insertion of alkynes. Furthermore, the alkyne insertion product, **5**, was found to undergo hydrogenation chemistry with H_2 (g) to reform the starting material, **2**, and hexane in 21% yield. While these reactivity studies are comparable to other tin(II) species that feature insertion of alkynes and oxidative addition at Sn; to our knowledge, we report the first example of tin(II) hydrogenation of the hydrostannylated alkyne.[34,42–44] This demonstrates a platform that may lead to catalytic applications for the Sn–H mediated hydrogenation of unsaturated organic molecules. Ongoing studies of **2**, **3**, **4** and **5** are focused on Mössbauer characterization, DFT modeling and further chemical reactivity experiments. Results will be reported separately.

Data availability

Crystallographic data for **2**, **3**, **4**, and **5** have been deposited at the CCDC under 2102266, 2173131, 2169137, 2169160, respectively.†

Author contributions

N. A. T. and C. P. K. conceived of the idea. N. A. T. developed the methodology. N. A. T. and Q. C. B. acquired the data for synthesis and characterization. N. A. T. and M. G. acquired and analysed the crystallographic data for compounds **2**, **3**, **4**, and **5**. J. M. P. and N. A. T. performed DFT studies for complex **2**. A. A. M. facilitated with NMR spectroscopic studies. N. A. T., T. C., and F. M. B. acquired and analysed electrochemical data. N. A. T. and C. P. K. wrote and edited the manuscript.

Conflicts of interest

There are no conflicts to declare.

Acknowledgements

N. A. T. acknowledges Micah Ziegler for invaluable discussions. N. A. T. acknowledges support from NSF for a Graduate Research Fellowship. Financial support from NSF is also gratefully acknowledged (CHE-1853908). The authors thank Theresa Block, Aylin Koldemir, and Rainer Pöttgen for Mössbauer investigations.

Notes and references

1 A. G. Davies, *Organotin chemistry*, John Wiley & Sons, 2006.
2 M. Pereyre, J.-P. Quintard and A. Rahm, *Tin in organic synthesis*, Butterworth-Heinemann, 2013.
3 E. Rivard, R. C. Fischer, R. Wolf, Y. Peng, W. A. Merrill, N. D. Schley, Z. Zhu, L. Pu, J. C. Fettinger, S. J. Teat, I. Nowik, R. H. Herber, N. Takagi, S. Nagase and P. P. Power, *J. Am. Chem. Soc.*, 2007, **129**, 16197–16208.
4 B. E. Eichler and P. P. Power, *J. Am. Chem. Soc.*, 2000, **122**, 8785–8786.
5 Y. Peng, B. D. Ellis, X. Wang and P. P. Power, *J. Am. Chem. Soc.*, 2008, **130**, 12268–12269.
6 S. Wang, M. L. McCrea-Hendrick, C. M. Weinstein, C. A. Caputo, E. Hoppe, J. C. Fettinger, M. M. Olmstead and P. P. Power, *J. Am. Chem. Soc.*, 2017, **139**, 6586–6595.
7 S. Wang, M. L. McCrea-Hendrick, C. M. Weinstein, C. A. Caputo, E. Hoppe, J. C. Fettinger, M. M. Olmstead and P. P. Power, *J. Am. Chem. Soc.*, 2017, **139**, 6596–6604.
8 J. Schneider, C. P. Sindlinger, K. Eichele, H. Schubert and L. Wesemann, *J. Am. Chem. Soc.*, 2017, **139**, 6542–6545.
9 E. Rivard and P. P. Power, *Dalton Trans.*, 2008, 4336–4343.
10 A. Jana, H. W. Roesky, C. Schulzke and P. P. Samuel, *Organometallics*, 2010, **29**, 4837–4841.
11 A. Jana, H. W. Roesky, C. Schulzke and A. Döring, *Angew. Chem., Int. Ed.*, 2009, **48**, 1106–1109.
12 T. J. Hadlington, M. Hermann, G. Frenking and C. Jones, *J. Am. Chem. Soc.*, 2014, **136**, 3028–3031.
13 O. T. Summerscales, C. A. Caputo, C. E. Knapp, J. C. Fettinger and P. P. Power, *J. Am. Chem. Soc.*, 2012, **134**, 14595–14603.
14 S. Wang, T. J. Sherbow, L. A. Berben and P. P. Power, *J. Am. Chem. Soc.*, 2018, **140**, 590–593.
15 A. V. Protchenko, J. I. Bates, L. M. A. Saleh, M. P. Blake, A. D. Schwarz, E. L. Kolychev, A. L. Thompson, C. Jones, P. Mountford and S. Aldridge, *J. Am. Chem. Soc.*, 2016, **138**, 4555–4564.
16 S. M. I. Al-Rafia, A. C. Malcolm, S. K. Liew, M. J. Ferguson and E. Rivard, *J. Am. Chem. Soc.*, 2011, **133**, 777–779.
17 S. M. I. Al-Rafia, O. Shynkaruk, S. M. McDonald, S. K. Liew, M. J. Ferguson, R. McDonald, R. H. Herber and E. Rivard, *Inorg. Chem.*, 2013, **52**, 5581–5589.
18 J.-J. Maudrich, M. Widemann, F. Diab, R. H. Kern, P. Sirsch, C. P. Sindlinger, H. Schubert and L. Wesemann, *Eur. J. Chem.*, 2019, **25**, 16081–16087.
19 Q. Zhu, J. C. Fettinger and P. P. Power, *Dalton Trans.*, 2021, **50**, 12555–12562.
20 M. M. D. Roy, A. A. Omaña, A. S. S. Wilson, M. S. Hill, S. Aldridge and E. Rivard, *Chem. Rev.*, 2021, **121**, 12784–12965.
21 S. M. I. Al-Rafia, A. C. Malcolm, R. McDonald, M. J. Ferguson and E. Rivard, *Angew. Chem., Int. Ed.*, 2011, **50**, 8354–8357.

22 P. P. Power, *Nature*, 2010, **463**, 171–177.
23 Q. Zhao, T. D. Harris and T. A. Betley, *J. Am. Chem. Soc.*, 2011, **133**, 8293–8306.
24 E. V. Eames and T. A. Betley, *Inorg. Chem.*, 2012, **51**, 10274–10278.
25 B. K. Breedlove, P. E. Fanwick and C. P. Kubiak, *Inorg. Chem.*, 2002, **41**, 4306–4308.
26 E. Simón-Manso and C. P. Kubiak, *Angew. Chem., Int. Ed.*, 2005, **44**, 1125–1128.
27 A. R. Leverett, V. Diachenko, M. L. Cole and A. I. McKay, *Dalton Trans.*, 2019, **48**, 13197–13204.
28 T. J. Hadlington, M. Hermann, J. Li, G. Frenking and C. Jones, *Angew. Chem., Int. Ed.*, 2013, **52**, 10199–10203.
29 V. M. S. Gil and W. Von Philipsborn, *Magn. Reson. Chem.*, 1989, **27**, 409–430.
30 B. Wrackmeyer, *Annual Reports on NMR Spectroscopy*, ed. G. A. Webb, Academic Press, 1999, vol. 38, pp. 203–264.
31 R. E. Wasylishen and N. Burford, *Can. J. Chem.*, 1987, **65**, 2707–2712.
32 C. P. Sindlinger and L. Wesemann, *Chem. Sci.*, 2014, **5**, 2739–2746.
33 L. W. Pineda, V. Jancik, K. Starke, R. B. Oswald and H. W. Roesky, *Angew. Chem., Int. Ed.*, 2006, **45**, 2602–2605.
34 M. J. S. Gynane, M. F. Lappert, S. J. Miles and P. P. Power, *J. Chem. Soc., Chem. Commun.*, 1976, 256–257.
35 A. C. Filippou, A. I. Philippopoulos and G. Schnakenburg, *Organometallics*, 2003, **22**, 3339–3341.
36 A. C. Filippou, D. Hoffmann and G. Schnakenburg, *Chem. Sci.*, 2017, **8**, 6290–6299.
37 J. D. Queen, A. C. Phung, C. A. Caputo, J. C. Fettinger and P. P. Power, *J. Am. Chem. Soc.*, 2020, **142**, 2233–2237.
38 M. Widemann, K. Eichele, H. Schubert, C. P. Sindlinger, S. Klenner, R. Pöttgen and L. Wesemann, *Angew. Chem., Int. Ed.*, 2021, **60**, 5882–5889.
39 A. C. Filippou, P. Ghana, U. Chakraborty and G. Schnakenburg, *J. Am. Chem. Soc.*, 2013, **135**, 11525–11528.
40 A. C. Filippou, P. Portius, A. I. Philippopoulos and H. Rohde, *Angew. Chem., Int. Ed.*, 2003, **42**, 445–447.
41 M. Alami, A. Hamze and O. Provot, *ACS Catal.*, 2019, **9**, 3437–3466.
42 M. L. McCrea-Hendrick, S. Wang, K. L. Gullett, J. C. Fettinger and P. P. Power, *Organometallics*, 2017, **36**, 3799–3805.
43 T. J. Hadlington, M. Hermann, G. Frenking and C. Jones, *Chem. Sci.*, 2015, **6**, 7249–7257.
44 S. K. Mandal and H. W. Roesky, *Acc. Chem. Res.*, 2012, **45**, 298–307.
45 K. Wade, *Chem. Commun.*, 1971, 792–793.
46 D. M. P. Mingos, *Nat. Phys. Sci.*, 1972, **236**, 99–102.